


Exact Short-Time Identification of Rational or Polynomial Exponent Signals

Shigeru Ando , *Life Member, IEEE*

Abstract—This paper describes a novel model and short-time estimation method of nonstationary or generalized sinusoids and their parameters. The model expresses the time derivative of log-amplitude and phase (complex exponent) with a rational function of time. When all poles of the rational function are simple, it is integrated to obtain the sum of polynomial and logarithm functions. The former generates a polynomial exponent signal, which is multiplied by an intensely time-varying function generated from the latter. Its direct estimator based on the weighted integral method provides an exact solution in the noiseless case from a small number of finite (short-time) Fourier coefficients; thus, multiple sinusoids separated in either the time domain or the frequency domain can be estimated independently. Several experimental tests of the basic performances are shown under possible application scenarios including the analog or digital AM/FM wave demodulation, radar/sonar pulse detection and parameterization, and combined uses of the proposed method with pulse compression.

Index Terms—Nonstationary sinusoid, direct algebraic method, polynomial phase, Chirp, period modulation, radar, Doppler.

I. INTRODUCTION

MODELING and estimation of nonstationary sinusoids are one of the oldest and still continuing research subjects in a wide range of signal processing fields including radar, sonar, communications, acoustics, and optics. Signals as the target of detection and analysis are often characterized by their own deterministic natures. Although there are advantages as well as disadvantages in parametric approaches, the aim of model-based approaches is to extract more widely and accurately these natures in order to understand and exploit the underlying phenomena using a shorter analysis window and an increased signal-to-noise ratio (SNR). Signals in communications and audio applications are complex mixture of amplitude-modulated (AM) and frequency-modulated (FM) components with rapidly varying amplitude and phase, which are sometimes too important to be neglected for their efficient, detailed, and fruitful analysis.

Polynomial phase (including log-amplitude) signal (PPS) models are the most fundamental and extensively studied ones. The estimation methods include recursive multiplication [1], phase unwrapping and linear regression [2], polynomial phase transform [3], [4], generalized ambiguity function [5], nonlinear

instantaneous least squares estimate [6], cubic or higher-order phase functions [7], [8], [9], [10], and distribution derivative method for closed form solutions [11], [12]. The PPSs, however, are not always sufficient to describe sudden transitions of real signals such as speech and music. Extensions of sinusoidal models have been explored including those of cyclostationary polynomial signals with random amplitude [13], the polynomial amplitude complex exponential (PACE) as the general solution of autoregressive model [14], gamma-enveloped sinusoids [15], the phase vocoder approach [16], and the coupled PPS and sinusoidal FM models [17], [18]. Models should be simple, mathematically tractable, and general for describing diversified signal components and for estimating parameters easily and accurately. Further preferable and unified models in this sense are still open issues.

Signals for radars, sonars, and diagnostic equipment are so designed to extract delay and Doppler information under constraints in signal power and varying propagation conditions. Theoretical analysis of the waveforms is based on the ambiguity functions. Chirp signals or PPSs with suitable envelopes are commonly used. For the decoupled detection of position and velocity, linear period modulation (LPM), also known as the hyperbolic chirp/FM, has been widely studied. Studies include those on the LPM as a Doppler-insensitive waveform [19], resemblance of it to bat signals [20], quadrature detection of range and velocity [21], use of multiple waveform sets for delay Doppler imaging [22], estimation of the product of hyperbolic FM and chirp signals [23], generalized analysis of coupled and uncoupled waveforms [24], and use of sub-band correlators [25]. Most of these methods rely on the matched filter array that requires the maximum search, but the interpolation in the finite search intervals often reduces the accuracies. An appropriate use of a model-based, direct estimation method will be desirable to systematically construct suitable waveforms and to extend their overall performances.

In recent years, a mathematical technique, the weighted integral method (WIM), for differential/difference model parameter identification from finite duration observation has been developed and applied to sinusoidal parameter estimation [26], [27], [28], localization of poles of meromorphic function [29], white light interferometry [30], [31], sound source localization [32], magnetic dipole localization [33], and algebraic solution of optical flow [34], [35], [36], [37]. The WIM relies on mostly linear signal generation models; thus, it is free from iterative nonlinear optimization owing to functional nonlinearities of signal waveforms. The length of the observation interval can

Manuscript received 7 February 2022; revised 28 September 2022; accepted 20 November 2022. Date of publication 25 November 2022; date of current version 6 December 2022. The associate editor coordinating the review of this manuscript and approving it for publication was Dr. Sheetal Kalyani.

The author is with the Professor Emeritus, University of Tokyo, Chiba 266-0031, Japan (e-mail: shigeru_ando@ipc.i.u-tokyo.ac.jp).

Digital Object Identifier 10.1109/TSP.2022.3224792

be arbitrarily chosen without any loss of exactness, and the edge effects at the boundaries are eliminated using model-originated extra unknowns or a properly designed windowing of model equations. The purpose of this study, which is based on the WIM, is to develop a simple but extended model of nonstationary sinusoids and the direct algebraic estimation method of its parameters. In the following sections, a differential equation (DE) model is introduced, its basic properties are described briefly, and the direct algebraic estimators of its coefficients are obtained. Then, experimental tests of the basic performances are shown under several application scenarios including the AM/FM demodulation, radar/sonar pulse detection and parameterization, mixture detection, and combined uses of the proposed method with pulse compression.

II. DIFFERENTIAL EQUATION MODELING

A. Nonstationary Sinusoidal Differential Equation (NSDE)

Let $f(t)$ be a complex continuous signal that is nonzero in the interval of interest. Then,

$$\frac{d}{dt} \log f(t) = \frac{\dot{f}(t)}{f(t)} = \dot{r}(t), \quad (1)$$

where $r(t)$ is a complex continuous function with its derivative $\dot{r}(t)$. By multiplying both sides of (1) by $f(t)$, and introducing a complex driving term $\xi(t)$, the nonstationary sinusoidal differential equation is expressed as

$$\dot{f}(t) - \dot{r}(t)f(t) = \xi(t) \quad (2)$$

with the general solution where $\xi(t) = 0$ and $f(t) \neq 0$ as

$$f(t) = Ae^{r(t)}, \quad (3)$$

where A is a complex amplitude, and $\Re r(t)$ and $\Im r(t)$ are the time-varying log-amplitude and phase, respectively. The driving term $\xi(t)$ is introduced to avoid a meaningless solution $f(t) = \dot{f}(t) = 0$ and to express a deviation from the ideal waveform due to noise. The physical meaning and existence condition of $\xi(t)$ as a driving term will be a subject of further consideration. In (3), the redundancies in A and $r(t)$ are removed by assuming $r(0) = 0$ at $t = 0$.

B. NSDE for Rational Exponent Signals

As the most vital part of the proposed models, consider the case where the differential exponent $\dot{r}(t)$ is a rational (including a polynomial) function of t expressed as

$$\dot{r}(t) = \frac{\sum_{i=0}^L b_i t^i}{\sum_{i=0}^K a_i t^i}, \quad (4)$$

where a_0, a_1, \dots, a_K and b_0, b_1, \dots, b_L are complex constants. Without loss of generality, we can assume $a_0 = 1$. Under this modeling, the NSDE is expressed as

$$\sum_{i=0}^K a_i t^i \dot{f}(t) - \sum_{i=0}^L b_i t^i f(t) = \xi(t), \quad (5)$$

which is the rational exponent differential equation (REDE). Although the integral of (4) includes log or arctan functions

generally, we call the general solutions of (5) the rational exponent signals.

If all poles z_i ($i = 1, \dots, K$) of the rational function of (4) are simple, $\dot{r}(t)$ can be decomposed as

$$\frac{\sum_{i=0}^L b_i t^i}{\sum_{i=0}^K a_i t^i} = P(t) + \sum_{i=1}^K \frac{\beta_i}{t - z_i}, \quad (6)$$

where $P(t)$ is the polynomial of order less than $L - K$, and β_i ($i = 1, \dots, K$) are complex constants. After integration, the signal has the form

$$\begin{aligned} f(t) &= A \exp \left\{ \int P(t) dt \right\} \cdot \prod_{i=1}^K e^{\beta_i \log(t - z_i)} \\ &= \left(A \prod_{i=1}^K (t - z_i)^{\beta_i} \right) \cdot \exp \left\{ \int P(t) dt \right\}, \end{aligned} \quad (7)$$

which can be seen as a polynomial exponent signal ($\exp\{\}$ term) modulated by a complex time-varying amplitude (product term). The product term in (7) or the fraction terms in (4) can describe localized and rapid changes of amplitude and phase near the poles. On the basis of the Weierstrass approximation theorem, the polynomial term with a sufficient order can approximate continuous distributions uniformly with a required accuracy. Hence, it is suitable for the parametric description of arbitrary waveforms in a finite interval. The rational modeling using (4) extends this capability with a smaller number of coefficients. Also, the rational exponent is a common property of various pulsed waves in radars, sonars, and diagnosis/inspection equipment. The product, time shift, and their time shrinkage/stretch are also rational exponent signals. Therefore, estimation of the coefficients of (4) is useful for the detection and analysis of those waves in a wide range of applications.

III. IDENTIFICATION OF RATIONAL EXPONENT SIGNALS

The problem here is the estimation of coefficients a_i ($i = 1, 2, \dots, K$) and b_i ($i = 0, 1, \dots, L$) from the observed signal $f(t)$ in a finite observation interval $[-T/2, T/2]$ so that (5) is satisfied in the least-squares sense. The observation interval is involved in an isolated duration of the signal.

A. Algebraic Equations of Fourier Coefficients

By introducing finite duration Fourier bases $\{e^{-jn\Delta_\omega t}\}$, where $\Delta_\omega \equiv 2\pi/T$, as a complete set of weight functions, we can equivalently express the condition for satisfying (5) in the interval as

$$\begin{aligned} \sum_{i=0}^K a_i t^i \dot{f}(t) - \sum_{i=0}^L b_i t^i f(t) &= \xi(t) \quad \forall t \in \left[-\frac{T}{2}, \frac{T}{2} \right] \\ \iff \int_{-T/2}^{T/2} \left\{ \sum_{i=0}^K a_i t^i \dot{f}(t) - \sum_{i=0}^L b_i t^i f(t) \right\} e^{-jn\Delta_\omega t} dt \\ &= \int_{-T/2}^{T/2} \xi(t) e^{-jn\Delta_\omega t} dt \quad \forall n. \end{aligned} \quad (8)$$

Let us express the weighted integrals of $f(t)$ as

$$g_n^{[i]} \equiv \int_{-T/2}^{T/2} t^i f(t) e^{-jn\Delta_\omega t} dt, \quad g_n^{[0]} \equiv g_n.$$

Note that no smooth window is introduced for removing edge effects. Then, by the integral by parts, the weighted integrals of $\dot{f}(t)$ are expressed as

$$\begin{aligned} & \int_{-T/2}^{T/2} t^i \dot{f}(t) e^{-jn\Delta_\omega t} dt \\ &= [f(t) t^i e^{-jn\Delta_\omega t}]_{-T/2}^{T/2} \\ & \quad - \int_{-T/2}^{T/2} f(t) (it^{i-1} - jn\Delta_\omega t^i) e^{-jn\Delta_\omega t} dt \\ &= \begin{cases} (T/2)^i (-1)^n F_- - ig_n^{[i-1]} + jn\Delta_\omega g_n^{[i]} & (i : \text{even}) \\ (T/2)^i (-1)^n F_+ - ig_n^{[i-1]} + jn\Delta_\omega g_n^{[i]} & (i : \text{odd}) \end{cases}, \end{aligned}$$

where

$$F_- \equiv f\left(\frac{T}{2}\right) - f\left(-\frac{T}{2}\right), \quad F_+ \equiv f\left(\frac{T}{2}\right) + f\left(-\frac{T}{2}\right) \quad (9)$$

are integral boundary terms. Fortunately, these terms do not dependent on the frequency order n and the power i of t except for the parity. Therefore, by denoting

$$F_0 = \sum_{i=0}^K a_i \left(\frac{T}{2}\right)^i F_{\mp:i}, \quad F_{\mp:i} \equiv \begin{cases} F_- & (i : \text{even}) \\ F_+ & (i : \text{odd}) \end{cases}, \quad (10)$$

we obtain the equivalent algebraic equations as

$$\begin{aligned} & (-1)^n F_0 - \sum_{i=1}^K a_i i g_n^{[i-1]} \\ & + jn\Delta_\omega \sum_{i=0}^K a_i g_n^{[i]} - \sum_{i=0}^L b_i g_n^{[i]} = \eta_n \quad \forall n, \end{aligned} \quad (11)$$

where

$$\eta_n \equiv \int_{-T/2}^{T/2} \xi(t) e^{-jn\Delta_\omega t} dt \quad (12)$$

is the Fourier coefficient of the driving term.

In (11), $g_n^{[i]}$ ($i = 0, 1, \dots, \max(K, L)$) are obtained from the wave data, $a_0 = 1$, and $a_1, a_2, \dots, a_K, b_0, b_1, \dots, b_L$ are unknowns, but F_0 involves instantaneous quantities which are not on the sample times of the sampled data. η_n will be zero when the waveform has sufficient purity in the observation interval. The role of η_n in this case is in the description of observation noise in $g_n^{[i]}$.

The use of hypothesized Schwartz functions as test functions [11] or as the window function of localized Fourier transforms [12] will eliminate F_+ and F_- . It introduces, however, considerable changes in all $g_n^{[i]}$. The WIM provides the elimination schemes and resultant equations according to the DE model of each problem.

B. Extra Unknown Method

In this method, we treat all unknowns including F_0 equally and simultaneously, and obtain them using a sufficient number of equations with different n so that the sum of squares of the driving term η_n is minimized. Assuming $a_0 = 1$, it is thus expressed as a linear optimization problem

$$\begin{aligned} & (a_1, a_2, \dots, a_K, b_0, b_1, \dots, b_L, F_0) \\ &= \arg \min \sum_n \left| (-1)^n F_0 - \sum_{i=0}^K a_i (ig_n^{[i-1]} - jn\Delta_\omega g_n^{[i]}) \right. \\ & \quad \left. - \sum_{i=0}^L b_i g_n^{[i]} \right|^2, \end{aligned} \quad (13)$$

where \sum_n indicates the summation among all n used in the minimization. The number of complex unknowns for the minimization is $K + L + 2$, whereas the equation is complex. Hence, the required number of equations is larger than or equal to $K + L + 2$. Not all n are necessary. This is very convenient in applications. By restricting the use of $g_n^{[i]}$ contributing to the waveform of interest, we can reduce interferences from different components as well as the computing costs. We refer to the extra unknown (XU) method using N_F equations as the $N_F \times XU$ method.

C. Windowing of Equation Method

Among the unknowns in (11), F_0 depends on the boundary values and noises of the waveform, but others do not. Firstly eliminating F_0 with the rapidly varying properties will facilitate the stabilization of succeeding numerical algorithms. The elimination of F_0 is equivalent to the relaxation of the original weight function $e^{-jn\Delta_\omega t}$ into $p(t)e^{-jn\Delta_\omega t}$, where $p(t)$ is the window function that satisfies $p(\pm T/2) = 0$ at boundaries. The necessary condition for (8) is expressed as

$$\begin{aligned} & \int_{-T/2}^{T/2} \left\{ \sum_{i=0}^K a_i t^i \dot{f}(t) - \sum_{i=0}^L b_i t^i f(t) \right\} p(t) e^{-jn\Delta_\omega t} dt \\ &= \int_{-T/2}^{T/2} \xi(t) p(t) e^{-jn\Delta_\omega t} dt \quad \forall n. \end{aligned} \quad (14)$$

Since the integral boundary terms vanish, it follows that

$$-\sum_{i=0}^K a_i (i\tilde{g}_n^{[i-1]} - jn\Delta_\omega \tilde{g}_n^{[i]} + \tilde{h}_n^{[i]}) - \sum_{i=0}^L b_i \tilde{g}_n^{[i]} = \tilde{\eta}_n \quad \forall n, \quad (15)$$

where

$$\tilde{g}_n^{[i]} \equiv \int_{-T/2}^{T/2} t^i f(t) p(t) e^{-jn\Delta_\omega t} dt, \quad \tilde{g}_n^{[0]} \equiv \tilde{g}_n,$$

$$\tilde{\eta}_n \equiv \int_{-T/2}^{T/2} \xi(t) p(t) e^{-jn\Delta_\omega t} dt,$$

$$\tilde{h}_n^{[i]} \equiv \int_{-T/2}^{T/2} t^i f(t) \dot{p}(t) e^{-jn\Delta_\omega t} dt, \quad \tilde{h}_n^{[0]} \equiv \tilde{h}_n.$$

By assuming $a_0 = 1$, we can express the minimization criterion of the driving term as

$$(a_1, a_2, \dots, a_K, b_0, b_1, \dots, b_L) \\ = \arg \min \sum_n \left| \sum_{i=0}^K a_i u_n^{[i]} + \sum_{i=0}^L b_i \tilde{g}_n^{[i]} \right|^2, \quad (16)$$

where

$$u_n^{[i]} \equiv i \tilde{g}_n^{[i-1]} - j n \Delta \omega \tilde{g}_n^{[i]} + \tilde{h}_n^{[i]}, \quad u_n^{[0]} \equiv u_n,$$

and \sum_n is the summation among all n used in the minimization. The problem is linear; thus, it has a closed-form solution with the normal equation

$$\begin{bmatrix} \sum_n |u_n^{[1]}|^2 & \cdots & \sum_n u_n^{[1]*} u_n^{[K]} & \sum_n u_n^{[1]*} \tilde{g}_n & \cdots \\ \vdots & \ddots & \vdots & \vdots & \ddots \\ \sum_n u_n^{[K]*} u_n^{[1]} & \cdots & \sum_n |u_n^{[K]}|^2 & \sum_n u_n^{[K]*} \tilde{g}_n & \cdots \\ \sum_n \tilde{g}_n^* u_n^{[1]} & \cdots & \sum_n \tilde{g}_n^* u_n^{[K]} & \sum_n |\tilde{g}_n|^2 & \cdots \\ \vdots & \ddots & \vdots & \vdots & \ddots \\ \sum_n \tilde{g}_n^{[L]*} u_n^{[1]} & \cdots & \sum_n \tilde{g}_n^{[L]*} u_n^{[K]} & \sum_n \tilde{g}_n^{[L]*} \tilde{g}_n & \cdots \\ \sum_n u_n^{[1]*} \tilde{g}_n^{[L]} \\ \vdots \\ \sum_n u_n^{[K]*} \tilde{g}_n^{[L]} \\ \sum_n \tilde{g}_n^* \tilde{g}_n^{[L]} \\ \vdots \\ \sum_n |\tilde{g}_n^{[L]}|^2 \end{bmatrix} \begin{bmatrix} a_1 \\ \vdots \\ a_K \\ b_0 \\ \vdots \\ b_L \end{bmatrix} = - \begin{bmatrix} \sum_n u_n^{[1]*} u_n \\ \vdots \\ \sum_n u_n^{[K]*} u_n \\ \sum_n \tilde{g}_n^* u_n \\ \vdots \\ \sum_n \tilde{g}_n^{[L]*} u_n \end{bmatrix}. \quad (17)$$

To solve Eq. (17), a number of equations larger than or equal to $K + L + 1$ are necessary. Note that, for calculating $\tilde{g}_n^{[i]}$ and $\tilde{h}_n^{[i]}$, two or more Fourier coefficients are required.

As a class of window functions, we use [26]

$$p(t) = \sum_{m=-[(M-1)/2]}^{[M/2]} P_m e^{jm\Delta\omega t} \left(-\frac{T}{2} \leq t \leq \frac{T}{2} \right),$$

which is the weighted sum of M -tuple basis functions $e^{jm\Delta\omega t}$ ($-[(M-1)/2] \leq m \leq [M/2]$) ($[\]$ indicates the floor function). So that $p(t)$ is real symmetric when M is odd, we assume $P_m = P_m^* = P_{-m}$. So that $p(-t)^* = p(t)$ when M is even, we assume $P_m = P_m^* = P_{-m+1}$. So that $p(t)$ is zero at the boundaries,

$$p\left(\pm \frac{T}{2}\right) = \sum_{m=-[(M-1)/2]}^{[M/2]} (-1)^m P_m = 0, \quad (18)$$

then, it follows that

$$\tilde{g}_n^{[i]} = \sum_{m=-[(M-1)/2]}^{[M/2]} P_m g_{n-m}^{[i]} \quad (19)$$

$$\tilde{h}_n^{[i]} = -j\Delta\omega \sum_{m=-[(M-1)/2]}^{[M/2]} m P_m g_{n-m}^{[i]} \quad (20)$$

This shows that $\tilde{g}_n^{[i]}$ and $\tilde{h}_n^{[i]}$ are obtained by convolutions with weights P_m and mP_m ($-[(M-1)/2] \leq m \leq [M/2]$) on the Fourier coefficients without windowing. An example of $p(t)$ for $M = 2$ ($P_0 = P_1 = 1$) is a half-duration cosine function

$$p(t) = 1 + e^{j\Delta\omega t} = 2 \cos\left(\frac{\Delta\omega t}{2}\right) e^{-j\Delta\omega t/2},$$

which eliminates F_0 by adding order n and $n+1$ equations. Another example for $M = 3$ ($P_{-1} = P_1 = 1/2$, $P_0 = 1$) is the Hann window

$$p(t) = \frac{1}{2} e^{-j\Delta\omega t} + 1 + \frac{1}{2} e^{j\Delta\omega t} = 1 + \cos(\Delta\omega t)$$

using a weighted sum of order $n-1$, n , and $n+1$ equations with weights $1/2$, 1 , and $1/2$, respectively. We refer to the windowing methods with $M = 2$ and $M = 3$ as the 2FW and 3FW methods, respectively. By increasing M so that the higher-order differentials of $p(t)$ are zero at the boundaries, we can obtain an enhanced interference reduction capability from adjacent sinusoids at a slight expense of statistical efficiency [26] and also with a close relationship with the distribution derivative methods [11], [12]. n should be chosen around a peak of \tilde{g}_n distribution. The 2FW and 3FW methods using N_F frequency orders are denoted as the $N_F \times 2FW$ and $N_F \times 3FW$ methods, respectively.

Remark: The statistical efficiency (smallness of error variance) is best in the maximum likelihood (ML) method, but it requires an iteration and is easily trapped into local minima. The proposed method, although it is not best in the ML sense, provides directly an algebraic solution close to the global minimum. A refined solution closer to the ML, if necessary, will be obtained shortly by starting the ML iteration from the proposed estimate.

D. Desired Conditions for Stable Solution

A general theory is difficult to obtain. Thus, we describe here some requirements for the stability of algorithms.

Let n_1, n_2, \dots, n_{N_F} be all n used in (16). Then, so that b_0, b_1, \dots, b_L are definite, the vectors $(\tilde{g}_{n_1}^{[i]}, \tilde{g}_{n_2}^{[i]}, \dots, \tilde{g}_{n_{N_F}}^{[i]})$ ($0 \leq i \leq L$) are desired to have at least $L+1$ linearly independent components. Defining $p(t) = 0$ outside of $[-T/2, T/2]$, let us express the Fourier transform of the windowed signal waveform as

$$F(\omega) \equiv \int_{-\infty}^{\infty} f(t) p(t) e^{-j\omega t} dt.$$

Then, it follows generally that

$$F^{(m)}(\omega) = \frac{d^m}{d\omega^m} F(\omega) = (-j)^m \int_{-\infty}^{\infty} t^m f(t) p(t) e^{-j\omega t} dt;$$

hence, the weighted integral has a form that

$$\tilde{g}_n^{[m]} = j^m F^{(m)}(n\Delta\omega), \quad (21)$$

which implies that from 0th- to L th-order differentials of the signal spectrum at frequencies $n_1\Delta\omega, n_2\Delta\omega, \dots, n_{N_F}\Delta\omega$ should have sufficiently rich variations for definiteness. This seems to be possible when the frequencies are chosen from around the largest

peak in an extent of large variations of the spectral distribution of a time-varying sinusoid.

When $f(t)$, which is modeled as a rational exponent signal, actually has a polynomial exponent in the observation interval, there exist c_0, c_1, \dots, c_M such that

$$\dot{f}(t) = \sum_{m=0}^M c_m t^m f(t) \quad \forall t \in \left[-\frac{T}{2}, \frac{T}{2}\right].$$

Then, it follows for all n that

$$u_n^{[i]} = - \int_{-T/2}^{T/2} t^i \dot{f}(t) p(t) e^{-jn\Delta_\omega t} dt = - \sum_{m=0}^M c_m \tilde{g}_n^{[i+m]},$$

which means $u_n^{[i]}$ satisfying $0 \leq i + M \leq L$ is linearly related to $\tilde{g}_n^{[i]}$ ($0 \leq i \leq L$); hence, the estimation matrix for (16) degenerates. This wave is, however, expressed truly by the rational exponent model when $a_1 = \dots = a_K = 0$ and $b_0 = c_0, \dots, b_M = c_M, b_{M+1} = \dots = b_L = 0$. Therefore, the use of suitable regularization for the minimum norm solution will provide such estimates and avoid the ill condition. An example is shown in Example 2 of Section IV-A.

E. Estimation of Amplitude/Phase Constant

Let the integral of rational exponent be

$$\int \frac{\sum_{i=0}^L b_i t^i}{\sum_{i=0}^K a_i t^i} dt = r(t) + C, \quad (22)$$

where $r(t)$ here is calculated using the estimated a_i ($0 \leq i \leq K$), b_i ($0 \leq i \leq L$), the partial fraction decomposition, and integrals such that $r(0) = 0$. To estimate the complex constant A of $f(t) = Ae^{r(t)}$, we evaluate numerically the Fourier coefficients of $e^{r(t)}$ as

$$R_n = \int_{-T/2}^{T/2} e^{r(t)} e^{-jn\Delta_\omega t} dt. \quad (23)$$

Using the results, we express the least-squares method as

$$\hat{A} = \arg \min_n \sum_n |AR_n - g_n|^2 \quad (24)$$

with the solution

$$\hat{A} = \frac{\sum_n R_n^* g_n}{\sum_n |R_n|^2}. \quad (25)$$

For the windowing of equation method, R_n and g_n should be those calculated with the window $p(t)$.

IV. APPLICATION ISSUES AND EXPERIMENTAL TESTS

In this section, the proposed method is described, assuming particular conditions of various signal processing applications. Detailed analysis or comparison with existing methods is not the aim here. The applications include 1) AM-FM wave demodulation of analog or digital signal waveforms and 2) detection and parametrization of polynomial or rational exponent pulses. In the following experiments, sampled data with the length N (integer) were used. All integrals from the sample sequence

were approximated using the ‘‘half sample shift two-sample extension’’ method described in [26].

A. Moving Estimate of Modulation Parameters

By the truncated Taylor expansion at $t = 0$, the exponent $\zeta(t) + j\phi(t)$ of time-varying sinusoid is expressed as

$$\dot{r}(t) \equiv \dot{\zeta}(t) + j\dot{\phi}(t) \simeq \sum_{i=0}^L \frac{t^i}{i!} \left(\zeta^{(i+1)}(0) + j\phi^{(i+1)}(0) \right),$$

hence,

$$b_i \simeq \frac{1}{i!} \left(\zeta^{(i+1)}(0) + j\phi^{(i+1)}(0) \right) \quad (0 \leq i \leq L) \quad (26)$$

provides an approximate of $(i + 1)$ th order differentials of the log-amplitude and phase at the center of the observation interval $[-T/2, T/2]$. To estimate them, the normal equation is composed of a block for b_0, b_1, \dots, b_L in (17). For AM-only or FM-only signals, the solution can be constrained to be real or imaginary. The number and set of n chosen should be larger than or equal to $L + 1$ or $(L + 1)/2$ so that the spectral peak and the lobe of the modulated wave are enclosed.

Example 1. Demodulation of FM wave: Parameters to be estimated are $\Im b_0$ (instantaneous frequency), $\Im b_1$ (frequency rate), and others at $t = 0$ (center of observation interval). The amplitude is assumed to be constant. Then, the normal equation (real) is obtained as

$$\begin{bmatrix} \sum_n |\tilde{g}_n|^2 & \Re \sum_n \tilde{g}_n^* \tilde{g}_n^{[1]} & \dots & \Re \sum_n \tilde{g}_n^* \tilde{g}_n^{[L]} \\ \Re \sum_n \tilde{g}_n^{[1]*} \tilde{g}_n & \sum_n |\tilde{g}_n^{[1]}|^2 & \dots & \Re \sum_n \tilde{g}_n^{[1]*} \tilde{g}_n^{[L]} \\ \vdots & \vdots & \ddots & \vdots \\ \Re \sum_n \tilde{g}_n^{[L]*} \tilde{g}_n & \Re \sum_n \tilde{g}_n^{[L]*} \tilde{g}_n^{[1]} & \dots & \sum_n |\tilde{g}_n^{[L]}|^2 \end{bmatrix} \begin{bmatrix} \Im b_0 \\ \Im b_1 \\ \vdots \\ \Im b_L \end{bmatrix} = \begin{bmatrix} \sum_n n \Delta_\omega |\tilde{g}_n|^2 - \Im \sum_n \tilde{g}_n^* \tilde{h}_n \\ \Re \sum_n n \Delta_\omega \tilde{g}_n^{[1]*} \tilde{g}_n - \Im \sum_n \tilde{g}_n^{[1]*} \tilde{h}_n \\ \vdots \\ \Re \sum_n n \Delta_\omega \tilde{g}_n^{[L]*} \tilde{g}_n - \Im \sum_n \tilde{g}_n^{[L]*} \tilde{h}_n \end{bmatrix}. \quad (27)$$

The number of n for summation N_F must be $N_F \geq (L + 1)/2$. Fig. 1 shows a numerical simulation result obtained using the 3rd order model and 2FW method ($T = N = 64$, $N_F = 5$). The FM wave (complex) is modulated by a constant frequency sinusoid with a linearly increasing amplitude, and 20% white Gaussian noise is added. In all coefficients, the rms estimation error indicated by the error bar is about three times larger than the CRLB (whole data usage in the observation interval). The relative error increases in proportion to the coefficient order. No dependences are seen on the frequency of its changes.

Example 2. Demodulation of digital QAM wave: The quadrature amplitude modulated (QAM) wave of a digital code sequence differs significantly from those of continuous analog signals. The wave segment for each code is a pure sinusoid, whereas steep discontinuities are present at their boundaries. Detection of code boundaries is important for the synchronous recovery of the carrier and digital codes.

Description of such a discontinuity requires higher-order terms. The use of a rational exponent model is beneficial in this

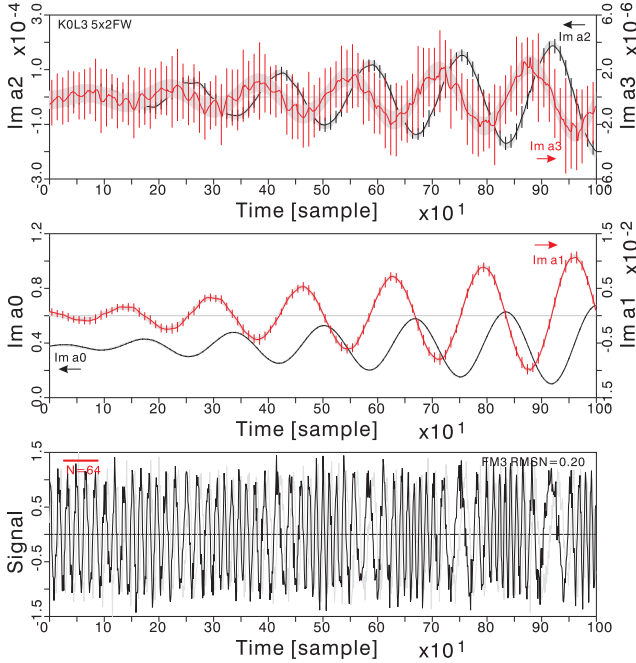


Fig. 1. Demodulation of FM wave with the imaginary-constraint 2FW method ($N = 64$, $N_F = 5$, 20% white Gaussian noise on the wave). The bottom graph is a noisy wave (complex), the middle graphs show the estimated values of $\Im a_0$ and $\Im a_1$, and the top graphs are those of $\Im a_2$ and $\Im a_3$. The vertical bars indicate the rms of estimation errors, and the thin gray zones indicate the error ranges determined by the CRLB around the true values.

respect since, for $|a_1 t| < 1$, it equivalently has a polynomial exponent

$$\begin{aligned} \frac{b_0 + b_1 t}{1 + a_1 t} &= (b_0 + b_1 t) (1 - a_1 t + a_1^2 t^2 - \dots) \\ &= b_0 + (b_1 - a_1 b_0)t - a_1(b_1 - a_1 b_0)t^2 \\ &\quad + a_1^2(b_1 - a_1 b_0)t^3 - \dots, \end{aligned}$$

which involves an infinite number of higher-order terms. The log-amplitude rate (LAR) and instantaneous frequency (IF) are expressed directly by b_0 . The higher-order terms compose a geometrical series with the common ratio and coefficient of $-a_1$ and $b_1 - a_1 b_0$, respectively.

The estimates of a_1 , b_0 , and b_1 are provided by (17) with $K = L = 1$. Fig. 2 shows a result for a 16QAM wave obtained using the rational-exponent 2FW method ($T = N = 64$, $N_F = 5$). In the bottom graph of a raw waveform (complex, 2% white Gaussian noise), periodic discontinuities are evident between codes. The estimates of $\Re b_0$ (LAR) and $\Im b_0$ (IF) are mostly zero and constant, respectively. Sharp antisymmetric spikes are evident in a_1 and b_1 at code boundaries. The top graphs show the demodulated I/Q components and the determinant of estimation matrix for a_1 , b_0 , and b_1 . The determinant reduces significantly in the code segment because the pure sinusoidal waveform there causes the degeneration. For recovering the I/Q components, the linearly increasing phase of the carrier must be suitably restored across the observation intervals.

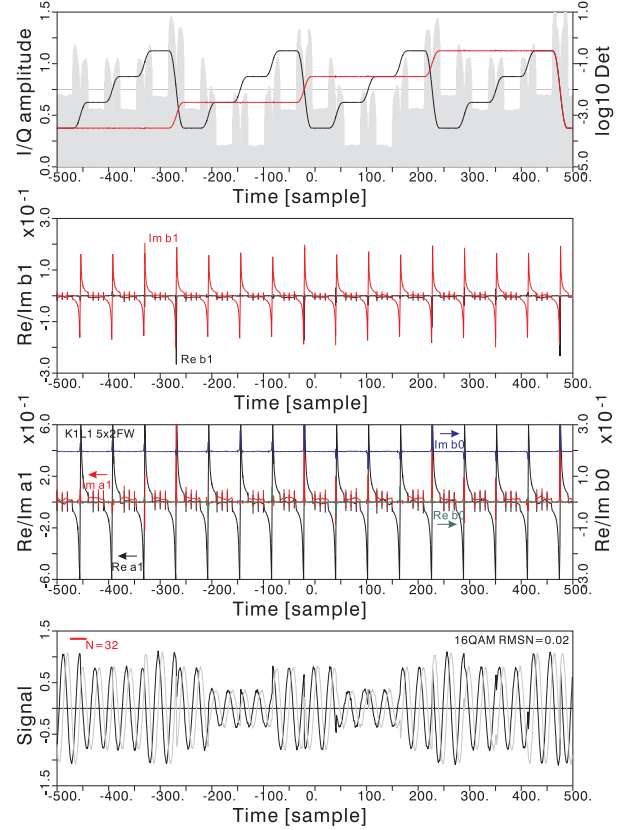


Fig. 2. Demodulation of digital quadrature-modulated (16QAM) wave with the rational-exponent 2FW method ($K = L = 1$, $N = 64$, $N_F = 5$, 2% white Gaussian noise is added on the wave). The bottom graph is an example of the noisy wave (complex), the middle low and high graphs are the estimated values of a_1 , b_0 and b_1 , respectively, and the top graphs are the demodulated amplitude and phase, and the log-determinant of the estimation matrix. The sharp spikes of a_1 , b_0 and b_1 are evident at the edges of digital codes. The vertical bars indicate the rms of estimation errors.

B. Parameterization of Nonstationary Sinusoidal Pulses

The nonstationary sinusoidal pulses are widely used in radar, sonar, and measurement systems for detecting various conditions during its propagation. Most typically, they undergo the propagation delay τ and the time scaling s owing to the Doppler effect. Using (6), we can express such a wave as

$$\begin{aligned} \frac{df(s(t - \tau))/dt}{f(s(t - \tau))} &= s \cdot \frac{\sum_{i=0}^L b_i s^i (t - \tau)^i}{\sum_{i=0}^K a_i s^i (t - \tau)^i} \\ &= sP(s(t - \tau)) + \sum_{i=1}^K \frac{\beta_i}{t - (\tau + z_i/s)}, \end{aligned}$$

which is still the rational exponent signal with the same order (K, L). It also shows increased and reduced dependences on s of the polynomial and the fraction terms, respectively. τ and s will be obtainable by comparing the known and estimated coefficients. The cross-correlation between 2nd-order polynomial exponent signals such as the Gabor pulse and chirped Gaussian pulse (CGP) is also the 2nd-order polynomial exponent signal. Therefore, the proposed estimation can be used after pulse

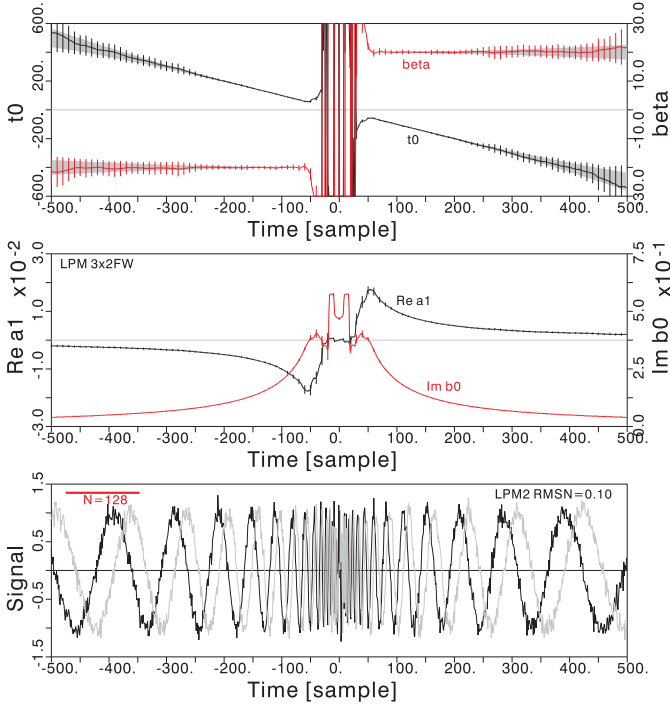


Fig. 3. Moving estimate of LPM wave with 2FW method ($K = L = 1$, $N = 128$, $N_F = 3$, and 10% white Gaussian noise is added on the wave). For $t < t_0$, the sign of β is inverted so that the phase rotation is positive. The bottom graph is a noisy wave (complex), the middle graphs are the estimated values of $\Re a_1$ and $\Im b_0$, and the top graphs are the estimated t_0 and β . The vertical bars across them indicate the rms of estimation errors, and the thin gray zones indicate the square roots of CRLB.

compression. These imply an extended range of applications of the parameter estimation approach.

The detection/parametrization will begin with the preliminary search and localization of the target pulse.

Example 3. Moving estimation of LPM wave: This wave is also called the hyperbolic chirp/FM. Let the time origin and phase coefficient be t_0 and β , respectively. Then, the wave $f(t) = Ae^{j\phi(t)} = Ae^{j\beta \log(t-t_0)}$ has the “period” $2\pi/\dot{\phi}(t) = 2\pi(t-t_0)/\beta$, which is proportional to time from the origin. It is thus time-scale-invariant except for its phase constant. The REDE for this wave is expressed as

$$-(t/t_0)\dot{f}(t) + \dot{f}(t) + j(\beta/t_0)f(t) = \xi(t), \quad (28)$$

where $\Re a_1 = -1/t_0$, $\Im b_0 = -\beta/t_0$ in (5). The normal equation (real) for minimizing the driving term is obtained as

$$\begin{bmatrix} \sum_n |u_n^{[1]}|^2 & \Im \sum_n u_n^{[1]} \tilde{g}_n^* \\ \Im \sum_n \tilde{g}_n^* u_n^{[1]} & \sum_n |\tilde{g}_n^{[1]}|^2 \end{bmatrix} \begin{bmatrix} \Re a_1 \\ \Im b_0 \end{bmatrix} = - \begin{bmatrix} \Re \sum_n u_n^{[1]*} u_n \\ \Im \sum_n \tilde{g}_n^* u_n \end{bmatrix}. \quad (29)$$

Fig. 3 shows a result obtained using the 2FW method ($N = 128$, $N_F = 3$). In the LPM signal (complex, 10% white Gaussian noise in both real and imaginary parts), the sign of β is reversed at $t < t_0$ so that the phase rotation is positive. Except for the central interval with an excessively high frequency, the

estimates of $\Re a_1$ and $\Im b_0$ and the calculated t_0 (time to the LPM origin from the center of observation interval) and β are appropriate. The rms errors of t_0 and β are about three times larger than those of the CRLB indicated by the gray zone around the true value.

Example 4. Estimation of LPM with Gaussian envelope: The Gaussian-enveloped LPM (GLPM) is used for the ranging and velocimetry of reflective objects. Let the parameters of the LPM phase be t_0 and β , and the origin and variance of the Gaussian envelope be $t_1 \gg t_0$ and σ^2 , respectively. Then, the waveform is expressed as

$$f(t) = Ae^{-(t-t_1)^2/2\sigma^2} e^{j\beta \log(t-t_0)};$$

thus, the time differential of the exponent has the form

$$\frac{\dot{f}(t)}{f(t)} = \frac{t_1/\sigma^2 - j\beta/t_0 - t(t_0 + t_1)/(t_0\sigma^2) + t^2/(t_0\sigma^2)}{1 - t/t_0},$$

which corresponds to the case in (4) when

$$\begin{aligned} a_1 &= -1/t_0, & b_0 &= t_1/\sigma^2 - j\beta/t_0 \\ b_1 &= -(t_0 + t_1)/(t_0\sigma^2), & b_2 &= 1/(t_0\sigma^2). \end{aligned}$$

The number of unknowns has increased from four to five for constructing the functional form of the rational exponent. The normal equation (real) for them is expressed as

$$\begin{bmatrix} \sum_n |u_n^{[1]}|^2 & \Re \sum_n u_n^{[1]*} \tilde{g}_n & \Im \sum_n u_n^{[1]} \tilde{g}_n^* & \Re \sum_n u_n^{[1]*} \tilde{g}_n^{[1]} \\ \Re \sum_n \tilde{g}_n^* u_n^{[1]} & \sum_n |\tilde{g}_n^{[1]}|^2 & 0 & \Re \sum_n \tilde{g}_n^* \tilde{g}_n^{[1]} \\ \Im \sum_n \tilde{g}_n^* u_n^{[1]} & 0 & \sum_n |\tilde{g}_n^{[1]}|^2 & \Im \sum_n \tilde{g}_n^* \tilde{g}_n^{[1]} \\ \Re \sum_n \tilde{g}_n^{[1]*} u_n^{[1]} & \Re \sum_n \tilde{g}_n^{[1]*} \tilde{g}_n & \Im \sum_n \tilde{g}_n^{[1]} \tilde{g}_n^* & \sum_n |\tilde{g}_n^{[1]}|^2 \\ \Re \sum_n \tilde{g}_n^{[2]*} u_n^{[1]} & \Re \sum_n \tilde{g}_n^{[2]*} \tilde{g}_n & \Im \sum_n \tilde{g}_n^{[2]} \tilde{g}_n^* & \Re \sum_n \tilde{g}_n^{[2]*} \tilde{g}_n^{[1]} \end{bmatrix} \begin{bmatrix} \Re a_1 \\ \Re b_0 \\ \Im b_0 \\ \Re b_1 \\ \Re b_2 \end{bmatrix} = - \begin{bmatrix} \Re \sum_n u_n^{[1]*} u_n \\ \Re \sum_n \tilde{g}_n^* u_n \\ \Im \sum_n \tilde{g}_n^* u_n \\ \Re \sum_n \tilde{g}_n^{[1]*} u_n \\ \Re \sum_n \tilde{g}_n^{[2]*} u_n \end{bmatrix}.$$

When all the waveform parameters are unknown, they are obtained using the relations

$$\begin{aligned} t_0 &= -1/\Re a_1, & \beta &= \Im b_0/\Re a_1 \\ \sigma^{-2} &= \Re a_1 \Re b_0 - \Re b_1, & t_1 &= \Re b_0/(\Re a_1 \Re b_0 - \Re b_1). \end{aligned}$$

Fig. 4 shows a moving estimation of GLPM with the 2FW method ($N = 128$, $N_F = 7$). The middle low graphs are the estimated values of $\Re a_1 = -1/t_0$, $\Re b_0 = t_1/\sigma^2$, and $\Im b_0 = -\beta/t_0$. The error variances are smallest for $\Re b_0$ and $\Im b_0$ (0th-order coefficients), and slightly larger for $\Re a_1$ (1st-order coefficient). Since $\Re a_1$ and $\Im b_0$ are proportional to the coefficient β , which is time-scale-invariant, $t_0 = \beta/\Im b_0$ provides a better estimate when β is known. The top graph shows the calculated results of GLPM parameters when all of them are unknown. Localization of the waveform origin t_1 is possible using t_0 plus a known offset $t_1 - t_0$ (phase-based estimate) or the zero cross of t_1 (amplitude-based). The estimates of t_0 and t_1 have similar accuracies under this condition of waveform.

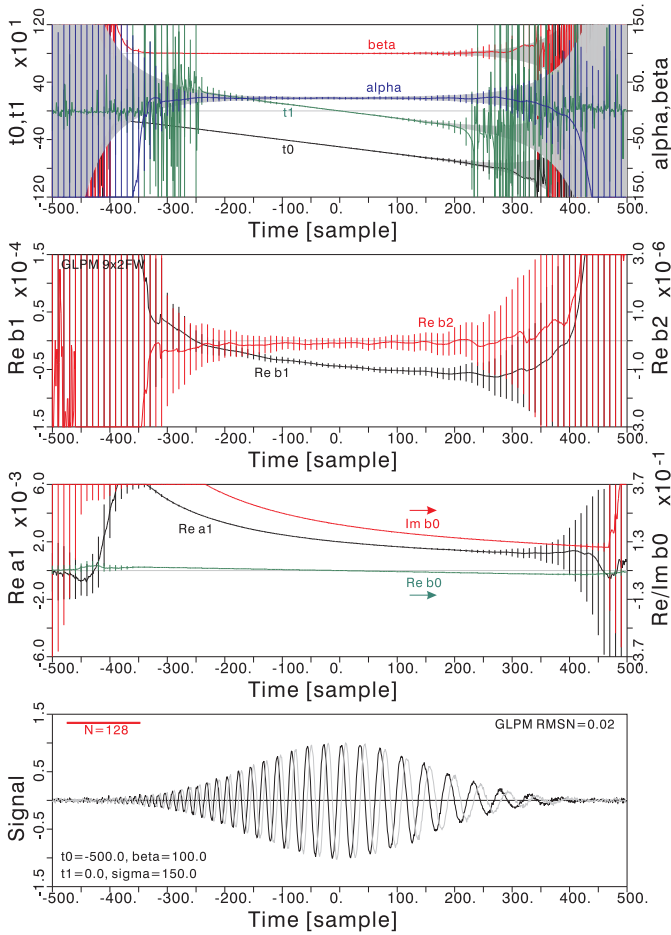


Fig. 4. Moving estimate of GLPM pulse with 2FW method ($K = 1, L = 2, N = 128, N_F = 7$, and 2% white Gaussian noise is added on the wave). The bottom graph is an example of a noisy wave (complex, origin is at the envelope peak), the middle low and high graphs are the estimated values of $\Re a_1, \Re b_0, \Im b_0$, and $\Re b_1, \Re b_2$, respectively, and the top graphs are the estimated t_0, t_1 (left-axis scale) and $\alpha \equiv 1/2\sigma^2$ and β (right axis scale, α is magnified 10^6 times). The vertical bars indicate the rms of estimation errors, and the thin gray zones indicate the CRLB.

They will vary according to the actual values, prior knowledge of GLPM parameters, and the presence/absence of a time scale change. After the moving estimates, extending the observation interval can further increase the accuracy.

In Figs. 5 and 6, the estimation error variances of $t_0 = -1/\Re a_1$ (LPM origin) at the waveform center $t = t_1 = 0$ are plotted in relation to the noise variance and the number of frequencies for the estimate, respectively. Fig. 5 shows that the 2FW method is stable under all conditions and has higher accuracy except in cases with small data length ($N = 64$ and $N = 128$). Its error variances are about 5 times larger than those of the CRLB in almost all cases. Note that it uses only $N_F \ll N$ frequencies although the CRLB assumes all data use in the observation interval. Differences among the three methods are caused by their different schemes of eliminating the integral boundary term. The extra unknown method shows higher accuracies for short data, but it shows an accuracy saturation under high-SNR conditions. Slightly increased error variances in the 3FW method are due to its smoother windowing.

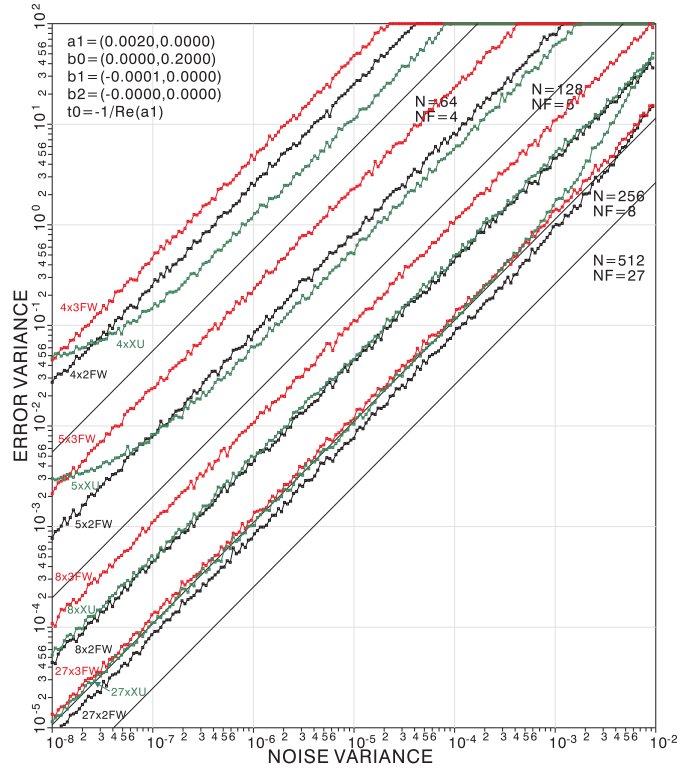


Fig. 5. Estimation error variances of $t_0 = -1/\Re a_1$ of the GLPM in Fig. 4 with the CRLB (thin black lines) using the rational exponent ($K = 1, L = 2$) 2FW method (black lines), 3FW method (red lines), and extra-unknown (XU) method (green lines). The data length and the number of frequencies for the estimate (N_F) are indicated near each CRLB line.

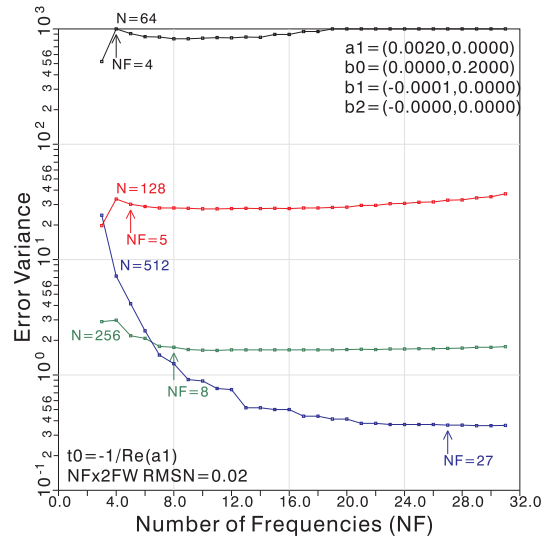


Fig. 6. Estimation error variance of GLPM parameters $t_0 = -1/\Re a_1$ in relation to the number of frequencies (N_F) around the spectral peak used for the estimation. Colored lines are for the observation length $N = 64$ (black), $N = 128$ (red), $N = 256$ (green), and $N = 512$ (blue).

Fig. 6 shows that the estimation error variances reach their minima at small N_F s and then increase gradually with the increase in N_F s. A method to determine an appropriate N_F is the calculation of the signal bandwidth estimated from the

span of IFs in the observation interval as

$$BW = - \left[\frac{\beta}{t - t_0} \right]_{-T/2}^{T/2} = \frac{\beta T}{t_0^2 - T^2/4} \quad (t \gg t_0).$$

Adding 4 to BW/Δ_ω for including the spectral sidelobe will be adequate for N_F . The values are indicated in Fig. 6.

C. Decision of Detection Based on Estimated Parameters

Usually, the target pulse is detected by matched filters including a possible variation of waveforms in templates followed by the maximum selection and thresholding. The threshold is determined from an expected noise level. In the proposed method, these operations correspond to the comparisons of 1) estimated parameters with their predetermined ranges and 2) the residual error of the estimated waveform with the noise level. For 2), the residual error in (24) expressed as

$$\sum_n |\hat{A}R_n g_n - g_n|^2 = \sum_n |g_n|^2 - \hat{A} \sum_n R_n g_n^* \quad (30)$$

can be compared with the expected value $2N_F T \sigma_f^2$, where $2\sigma_f^2$ and $2T\sigma_f^2$ are the noise variance of f and g_n , respectively, and N_F is the number of n used in the minimization.

D. Use Under Multipath Condition With Pulse Compression

The sum of rational exponent signals no longer satisfies their own REDEs. Thus, its estimation requires the isolated waveforms in the frequency domain or the time domain. For a delayed sum due to multipaths or clutters, satisfaction of this condition is very difficult. The matched filter, in contrast, is linear and maintains the additivity of signals; hence, it is extremely advantageous for use under such a condition. To extend the use of the parametric approach, we consider here some techniques for 1) superposition detection of nonstationary sinusoidal pulses and 2) combined use with pulse compression for superposition reduction.

Example 5. Measures of superposition of CGPs: The CGP is widely used for ranging and Doppler velocimetry. Detection of the superposed condition is important for the reliable use of the proposed method. The CGP waveform is expressed as

$$f(t) = A e^{-(t-t_1)^2/2\sigma^2 + j\beta(t-t_0)^2},$$

thus, the time-differential of exponent has a form

$$\frac{\dot{f}(t)}{f(t)} = t_1/\sigma^2 - 2j\beta t_0 - (1/\sigma^2 - 2j\beta)t,$$

which corresponds to the case in (4) when

$$b_0 = t_1/\sigma^2 - 2j\beta t_0, \quad b_1 = -1/\sigma^2 + 2j\beta$$

with the center frequency $\omega_0 = 2\beta(t_1 - t_0)$ at $t = t_1$.

Possible measures to detect the superposition will be the residual error in the amplitude/phase estimation (30) and the power of higher-order coefficients beyond the expected one. Fig. 7 shows the residual error and the higher-order polynomial coefficients of the 1st CGP at the center related to the displacement and relative amplitude of the 2nd CGP. The 2FW method

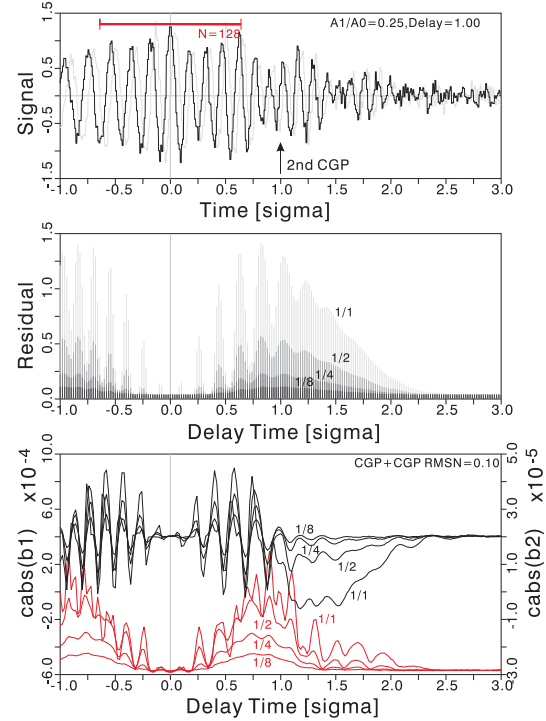


Fig. 7. Increase in residual error and generation of higher-order polynomial coefficients in the delayed sum of CGPs ($N = 128$, $N_F = 9$, 10% white Gaussian noise is added). The lateral axes are the delay time normalized by the variance of Gaussian envelope. The top graph shows the mixed waveform for the delay time σ and the amplitude ratio 1/4 of two CGPs. The bottom graphs show the averaged estimates of $|b_1|$ and $|b_2|$ when the amplitude ratios of the delayed CGP are 1, 1/2, 1/4, and 1/8.

($N = 128$, $N_F = 9$) is used and 10% white Gaussian noise is added. The anomalous response of b_1 (envelope curvature and chirp rate) is significant in the 0 to 2σ range of delay. Both the residual error and the excess-order coefficient increase their values in this delay range and become largest at about σ . For the application of the proposed method to the superposed CGPs in this example, this shows that at least an $\sim 2\sigma$ separation between them is required.

Example 6. Detection of CGPs with pulse compression: With pulse compression, the CGP obtains an enhanced signal energy and temporal resolution from distributed frequency components in the long envelope. In addition, the cross-correlation of different CGPs is the CGP, and autocorrelation of CGP reduces to the Gabor function, both of which can be identified directly using the proposed method.

Fig. 8 shows the moving parameter estimation of CGPs (up-chirp) with a multipath distortion and 20% white Gaussian noise using the 2FW method ($K = 0$, $L = 1$, $N = 128$, $N_F = 9$). Two CGPs have 1.6σ separation ($\sigma = 100$) and equal amplitudes. The middle low and high graphs are the estimated values of $\Im b_0$ (IF), $\Im b_1$ (frequency rate), $\Re b_0$ (LAR), and $\Re b_1$ (log-amplitude curvature), and the top graph is the measures of superposition used in Example 6. The rms estimation errors of the estimates and the scatters of the superposition measures are indicated by the vertical bars. The CRLB is indicated by the gray zones. The results show that both the zero crosses of $\Re b_0$

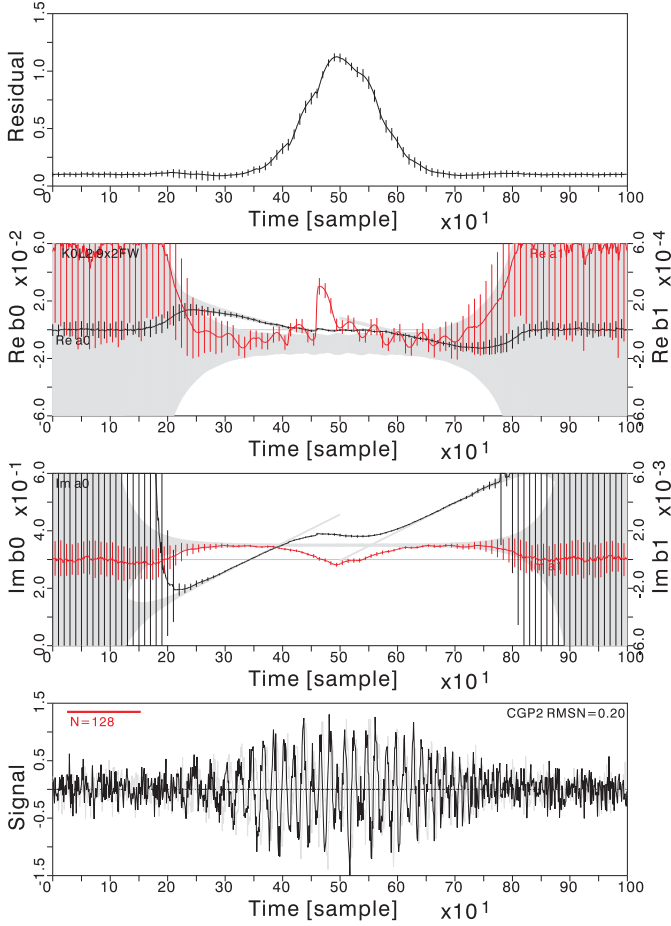


Fig. 8. Moving estimate of CGP with multipath distortion using 2FW method ($K = 0$, $L = 1$, $N = 128$, $N_F = 9$, 20% white Gaussian noise on the wave). The bottom graph is a noisy wave (complex) of superposed CGPs with 1.6σ separation ($\sigma = 100$) and equal amplitudes. The middle low graphs are the estimated $\Im b_0$ (IF, black line) and $\Im b_1$ (frequency rate, red line), the middle high graphs are the estimated $\Re b_0$ (log-amplitude rate, black line) and $\Re b_1$ (log-amplitude curvature, red line), and the top graph is the squared residual error in the amplitude/phase estimation. The vertical bars across them indicate the rms of estimation errors or scatters, and the gray zones indicate the CRLB.

and ω_0 crosses of $\Im b_0$ of the 1st and 2nd CGPs become unclear and biased, and the estimates become more anomalous near the center of two CGPs. These situations are also indicated by the increase in residual error in the amplitude/phase estimates as a superposition measure.

Fig. 9 shows the results after matched filtering. The compressed wave shown in the bottom graph provides enhanced separation and SNR. As shown in middle low and high graphs, the values of $\Im b_0$ (IF) and $\Im b_1$ (frequency rate) become constant (ω_0 and 0, respectively), whereas those of $\Re b_0$ (LAR) and $\Re b_1$ (log-amplitude curvature) increase and shorten the interference at the center; hence, the determination of zero crosses and increased curvatures at these crosses can be more accurate. In addition to the noise reduction via the matched filtering, significant reduction in estimation error of waveform parameters will be evident. The resolution of pulses and the improvement of the situation are also indicated by the drops of superposition measures at the matched-filter-output peaks in the top graph of Fig. 9.

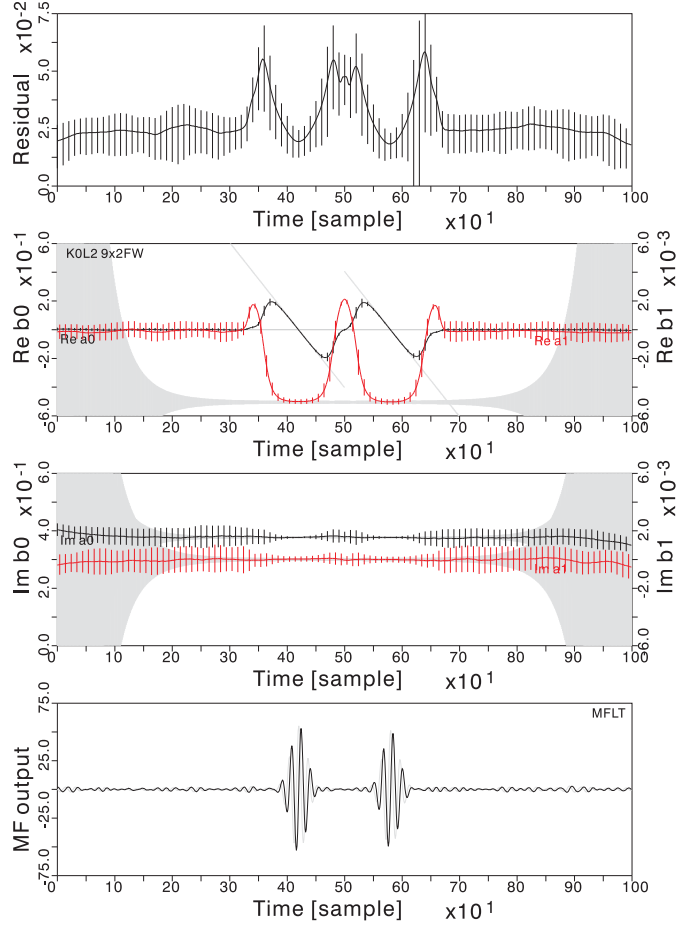


Fig. 9. Results of experiment in Fig. 8 after matched filtering (MF). The bottom graph shows the compressed wave after matched filtering. The middle low and middle high graphs are the estimated values of $\Im b_0$ and $\Im b_1$, and $\Re b_0$ and $\Re b_1$, respectively. The top graph is the squared residual error in the amplitude/phase estimation. The vertical bars along them indicate the rms of estimation errors or scatters, and gray zones indicate the CRLB around the true values.

V. SUMMARY AND CONCLUSION

In this paper, the rational exponent differential equation was introduced as a nonstationary sinusoidal model. It was then applied the weighted integral method to obtain the direct algebraic method to estimate its parameters. Experimental tests were performed to evaluate the basic performances of the proposed method under several possible application-specific conditions including AM/FM demodulation, radar/sonar pulse detection and parameterization, and combined uses of the proposed method with the multipath detection and pulse compression. They all showed extended and promising performances.

As a future work, it is desired to obtain relevant theories and algorithms for reliable applications of the proposed method to actual problems. They will include some modification to decrease the error variances toward the CRLB and methods for determining suitable model orders K and L for unknown time-varying sinusoids and an adequate observation length N and a number of frequency orders N_F used for the estimation.

REFERENCES

- [1] A. Nuttall, "Efficient evaluation of polynomials and exponentials of polynomials for equispaced arguments," *IEEE Trans. Acoust., Speech, Signal Process.*, vol. 35, no. 10, pp. 1486–1487, Oct. 1987.
- [2] P. M. Djuric and S. M. Kay, "Parameter estimation of chirp signals," *IEEE Trans. Acoust., Speech, Signal Process.*, vol. 38, no. 12, pp. 2118–2126, Dec. 1990.
- [3] S. Peleg and B. Porat, "Estimation and classification of polynomial-phase signals," *IEEE Trans. Inform. Theory*, vol. 37, no. 2, pp. 422–430, Mar. 1991.
- [4] S. Peleg and B. Friedlander, "The discrete polynomial-phase transform," *IEEE Trans. Signal Process.*, vol. 43, no. 8, pp. 1901–1914, Aug. 1995.
- [5] S. Barbarossa and V. Petrone, "Analysis of polynomial-phase signals by the integrated generalized ambiguity function," *IEEE Trans. Signal Process.*, vol. 45, no. 2, pp. 316–327, Feb. 1997.
- [6] J. Angeby, "Estimating signal parameters using the nonlinear instantaneous least squares approach," *IEEE Trans. Signal Process.*, vol. 48, no. 10, pp. 2721–2732, Oct. 2000.
- [7] P. O'Shea, "A new technique for instantaneous frequency rate estimation," *IEEE Signal Process. Lett.*, vol. 9, no. 8, pp. 251–252, Aug. 2002.
- [8] M. Farquharson and P. O'Shea, "Extending the performance of the cubic phase function algorithm," *IEEE Trans. Signal Process.*, vol. 55, no. 10, pp. 4767–4774, Oct. 2007.
- [9] P. Wang, I. Djurovic, and J. Yang, "Generalized high-order phase function for parameter estimation of polynomial phase signal," *IEEE Trans. Signal Process.*, vol. 56, no. 7, pp. 3023–3028, Jul. 2008.
- [10] I. Djurovic, M. Simeunovic, S. Djukanovic, and P. Wang, "A hybrid CPF-HAF estimation of polynomial-phase signals: Detailed statistical analysis," *IEEE Trans. Signal Process.*, vol. 60, no. 10, pp. 5010–5023, Oct. 2012.
- [11] M. Betsler, "Sinusoidal polynomial parameter estimation using the distribution derivative," *IEEE Trans. Signal Process.*, vol. 57, no. 12, pp. 4633–4645, Dec. 2009.
- [12] D. Fourer, F. Auger, K. Czarnecki, S. Meignen, and P. Flandrin, "Chirp rate and instantaneous frequency estimation: Application to recursive vertical synchrosqueezing," *IEEE Signal Process. Lett.*, vol. 24, no. 11, pp. 1724–1728, Nov. 2017.
- [13] S. Shamsunder, G. B. Giannakis, and B. Friedlander, "Estimating random amplitude polynomial phase signals: A cyclostationary approach," *IEEE Trans. Signal Process.*, vol. 43, no. 2, pp. 492–505, Feb. 1995.
- [14] R. Badeau, B. David, and G. Richard, "High-resolution spectral analysis of mixtures of complex exponentials modulated by polynomials," *IEEE Trans. Signal Process.*, vol. 54, no. 4, pp. 1341–1350, Apr. 2006.
- [15] M. G. Christensen and S. V. D. Par, "Efficient parametric coding of transients," *IEEE Trans. Audio Speech Lang. Process.*, vol. 14, no. 4, pp. 1340–1351, Jul. 2006.
- [16] M. Betsler, P. Collen, G. Richard, and B. David, "Estimation of frequency for AM/FM models using the phase vocoder framework," *IEEE Trans. Signal Process.*, vol. 56, no. 2, pp. 505–517, Feb. 2008.
- [17] P. Wang, P. V. Orlik, K. Sadamoto, W. Tsujita, and F. Gini, "Parameter estimation of hybrid sinusoidal FM-polynomial phase signal," *IEEE Signal Process. Lett.*, vol. 24, no. 1, pp. 66–70, Jan. 2017.
- [18] I. Djurovic, P. Wang, M. Simeunovic, and P. V. Orlik, "Parameter estimation of coupled polynomial phase and sinusoidal FM signals," *Signal Process.*, vol. 149, pp. 1–13, Aug. 2018.
- [19] J. J. Kroszczynski, "Pulse compression by means of linear-period modulation," *Proc. IEEE*, vol. 57, no. 7, pp. 1260–1266, Jul. 1969.
- [20] R. A. Altes and E. L. Titlebaum, "Bat signals as optimally doppler tolerant waveforms," *J. Acoust. Soc. Amer.*, vol. 48, no. 4, pp. 1014–1020, 1970.
- [21] R. A. Altes and D. P. Skinner, "Sonar velocity resolution with a linear-period-modulated pulse," *J. Acoust. Soc. Amer.*, vol. 61, no. 4, pp. 1019–1030, 1977.
- [22] J.-C. Guey and M. R. Bell, "Diversity waveform sets for delay-Doppler imaging," *IEEE Trans. Inform. Theory*, vol. 44, no. 4, pp. 1504–1522, Jul. 1998.
- [23] O. Besson, G. B. Giannakis, and F. Gini, "Improved estimation of hyperbolic frequency modulated chirp signals," *IEEE Trans. Signal Process.*, vol. 47, no. 5, pp. 1384–1388, May 1999.
- [24] Y. Doisy, L. Deruaz, S. P. Beerens, and R. Been, "Target Doppler estimation using wideband frequency modulated signals," *IEEE Trans. Signal Process.*, vol. 48, no. 5, pp. 1213–1224, May 2000.
- [25] P. R. Atkins, T. Collins, and K. G. Foote, "Transmit signal design and processing strategies for sonar target phase measurement," *IEEE J. Sel. Topics Signal Process.*, vol. 1, no. 1, pp. 91–104, Jun. 2007.
- [26] S. Ando and T. Nara, "An exact direct method of sinusoidal parameter estimation derived from finite Fourier integral of differential equation," *IEEE Trans. Signal Process.*, vol. 57, no. 9, pp. 3317–3329, Sep. 2009.
- [27] S. Ando, "Frequency-domain Prony method for autoregressive model identification and sinusoidal parameter estimation," *IEEE Trans. Signal Process.*, vol. 68, pp. 3461–3470, 2020.
- [28] S. Ando, "Time-frequency representation with variant array of frequency-domain Prony estimators," *J. Acoust. Soc. Amer.*, vol. 150, no. 4, pp. 2682–2694, 2021.
- [29] T. Nara and S. Ando, "Direct localization of poles of meromorphic function from measurements on incomplete boundary," *Inverse Problems*, vol. 26, 2010, Art. no. 015011.
- [30] S. Sato and S. Ando, "Weighted integral method in white-light interferometry: Envelope estimation from fraction of interferogram," in *Proc. SPIE Eur. Opt. Metrol.* 2009, vol. 7389, pp. 893–900.
- [31] S. Sato, T. Kurihara, and S. Ando, "Direct localization algorithm of white-light interferogram center based on the weighted integral method," *Trans. Soc. Instrum. Control Eng.*, vol. 46, no. 9, pp. 539–546, 2010.
- [32] S. Ando, T. Nara, and T. Levy, "Partial differential equation-based localization of a monopole source from a circular array," *J. Acoust. Soc. Amer.*, vol. 134, no. 4, pp. 2799–2813, 2013.
- [33] Y. Higuchi, T. Nara, and S. Ando, "Complete set of partial differential equations for direct localization of a magnetic dipole," *IEEE Trans. Magn.*, vol. 52, no. 5, May 2016, Art. no. 4000910.
- [34] S. Ando, W. Dabi, and P. Masurel, "Optical flow detection via complex-sinusoidally modulated imaging and its realization with correlation image sensor," *Trans. Inform. Process. Soc. Jpn.*, vol. 49, no. 6, pp. 13–21, 2008.
- [35] S. Ando, T. Nara, and T. Kurihara, "Spatial filtering velocimetry revisited: Exact short-time detecting schemes from arbitrarily small-size reticles," *Meas. Sci. Technol.*, vol. 25, no. 8, 2014, Art. no. 085001.
- [36] S. Ando, M. Nagase, T. Watanabe, T. Kosugi, and T. Iida, "Correlation image sensor for algebraic solution of optical flow," *IEEE J. Electron Devices Soc.*, vol. 9, pp. 170–179, 2021.
- [37] S. Ando and T. Kindo, "Direct imaging of stabilized optical flow and possible anomalies from moving vehicle," *IEEE Trans. Intell. Transport. Syst.*, early access, Aug. 26, 2022, doi: [10.1109/TITS.2022.3199203](https://doi.org/10.1109/TITS.2022.3199203).



Shigeru Ando (Life Member, IEEE) received the B.E., M.E., and Dr. Engr. degrees in mathematical engineering and information physics from the University of Tokyo, Tokyo, Japan, in 1974, 1976, and 1979, respectively. He was with the Faculty of Engineering of the University of Tokyo in 1979, an Associate Professor in 1987, a Professor from 1995 to 2016, and is currently a Professor emeritus with the Department of Mathematical Engineering and Information Physics, and the Department of Information Physics and Computing, University of Tokyo. His research interests include image processing, signal processing, inverse problems, optical and acoustic sensing, and bio-inspired visual, auditory, and tactile sensor devices.